PERGAMON

International Journal of Solids and Structures 39 (2002) 213–224

INTERNATIONAL JOURNAL OF SOLIDS and STRUCTURES

www.elsevier.com/locate/ijsolstr

Tensile response of ductile α-titanium at moderately high strain rates

J.M. Yuan, V.P.W. Shim *

Impact Mechanics Laboratory, Department of Mechanical Engineering, National University of Singapore, Singapore 119260, Singapore

Received 25 July 2000; in revised form 27 July 2001

Abstract

The tensile behavior of Grade 2 α-titanium is characterized for static loading and at moderately high strain rates (200–1000 s^{-1}). An experimental method is proposed to introduce sufficiently long tensile pulses to induce fracture in ductile specimens by incorporating a sacrificial fracture piece of adequately large diameter into a pendulum-driven tensile Kolsky bar. It is established that flow stress increases with strain rate. Necking in α-titanium occurs much earlier at high strain rates compared to static loading and results in significantly smaller necking and fracture strains. An equation describing the influence of strain rate and temperature softening on necking (tensile instability) is derived. The true stress–strain response between necking and fracture is estimated by measuring the final reduction in cross-sectional area. Fracture in specimens was observed using an optical microscope, which revealed typical ductile fracture characteristics.

Keywords: High strain rate; Tensile; α-titanium; Necking; Pendulum-driven tensile Kolsky bar

1. Introduction

Commercially pure Grade 2 α-titanium offers good weldability, superior corrosion resistance and a good balance between moderate strength and ductility. Examples of typical applications include airframe skins, aerospace structural components, heat exchangers, items in chemical processing plants and marine equipment parts. The use of titanium in situations where it is subjected to high-speed deformation necessitates an understanding of its dynamic behavior, to ensure that it can accommodate the stresses induced.

Meyers et al. (1994) studied shear band formation in α-titanium and observed extensive twining during high rate deformation of the material; they suggested that twinning could contribute to the initiation of shear bands. By using a servo-hydraulic testing machine, Kailas et al. (1993, 1994a,b) examined the plastic flow of α-titanium at strain rates up to 100 s^{-1} and at temperatures ranging from 25 °C to 400 °C. They

* Corresponding author. Tel.: +65-814-2228; fax: +65-779-1459.
E-mail address: mpespwv@nus.edu.sg (V.P.W. Shim).

0020-7683/01/$ - see front matter
PII: S0020-7683(01)00214-1

observed intense adiabatic shear banding in specimens deformed by compression at high strain rates. However, deformation was characterized by inhomogeneous flow due to plastic instability at lower strain rates. Chichili et al. (1998) performed dynamic compression tests on α-titanium at strain rates up to 6000 s^{-1} and found that the effective flow stress increased with strain rate. Also, the material appeared to be more rate sensitive at the highest strain rates investigated. The stress–strain curves indicated pronounced strain hardening behavior, with the degree of strain hardening increasing significantly with both strain rate and strain. Work on characterization of the dynamic tensile response of titanium is relatively limited, compared to studies involving dynamic compression. Harding (1975) obtained tensile stress–strain curves for α-titanium at five temperatures ranging from 77 to 298 K and at strain rates spanning 10^{-3} to 2.5×10^3 s^{-1}. From his results, he concluded that the activation enthalpy in the region of low rate sensitivity is a function of both stress and temperature, implying that multiple deformation mechanisms are active.

The preceding studies on the rate-dependent behavior of α-titanium focused on two regimes—low (<100 s^{-1}) and high (>1000 s^{-1}) strain rates; however, the dynamic characteristics of titanium at moderately high strain rates ranging from 100 to 1000 s^{-1} appears to be relatively scarce in published literature, especially for tensile loading. One major reason for this is the difficulty in performing dynamic tensile tests at moderately high strain rates on ductile materials like α-titanium.

The dynamic behavior of materials in the strain rate range of 10^2–10^4 s^{-1} has been widely studied using split Kolsky bars (Kolsky, 1949). This technique, initially used to load specimens in compression, has subsequently been modified to apply tension via various methods (Lindholm and Yeakley, 1981; Nicholas, 1981; Harding and Welsh, 1983; Staab and Gilat, 1991). A cylindrical striker is typically used to generate a tensile loading pulse in such testers (Lindholm and Yeakley, 1981; Nicholas, 1981; Harding and Welsh, 1983) and consequently, the pulse duration is dictated by the striker length. Staab and Gilat (1991) introduced a direct-tension split-Hopkinson-bar apparatus, whereby a load duration of 500 μs was generated by the release of elastic energy stored in a section of the input bar. Kawata et al. (1979) devised a single-bar system to achieve dynamic fracture in tough or ductile materials by using a pendulum to effect direct impact on a block connected to the specimen.

A tensile loading pulse of relatively long duration (estimated to be about 800 μs for a steel bar) is needed for dynamic tests on ductile titanium at moderately high strain rates of 100–1000 s^{-1}. In this study, a method for generating such pulses is established by incorporating the fracture of a short sacrificial rod into a pendulum-driven tensile Kolsky bar. The tensile response of Grade 2 α-titanium is investigated for static loading and at strain rates between 100 and 1000 s^{-1}; fracture in the specimens is examined using an optical microscope. From experimental observations, the flow stress mechanism, tensile instability and fracture characteristics of the material under moderately high strain rates are identified.

2. Experimental tests

2.1. Experimental technique and calibration test

Fig. 1 shows a schematic diagram of the pendulum-driven Kolsky bar used for applying dynamic tension at moderately high strain rates to titanium of high ductility. The input and output bars were made of high strength steel and measured 12.7 mm in diameter and 3 m in length. The incident and transmitted strain waves in the bars were monitored by strain gages located as shown in Fig. 1. A pair of 120 Ω (Kyowa KFG-2-120-C1-11) 2 mm axial gauges were placed at each location, on opposite sides of the bars. These gages, along with another two 120 Ω dummy gauges for each location, were used to complete a full Wheatstone bridge. Signals from the bridges were amplified by (Tokyo Sokki DC-92D) dynamic signal conditioners and stored on a (Yokogawa DL1540) digital oscilloscope; these were subsequently transferred to a computer for data processing. To ensure the absence of bending waves in the bars, the two gauges at each location were

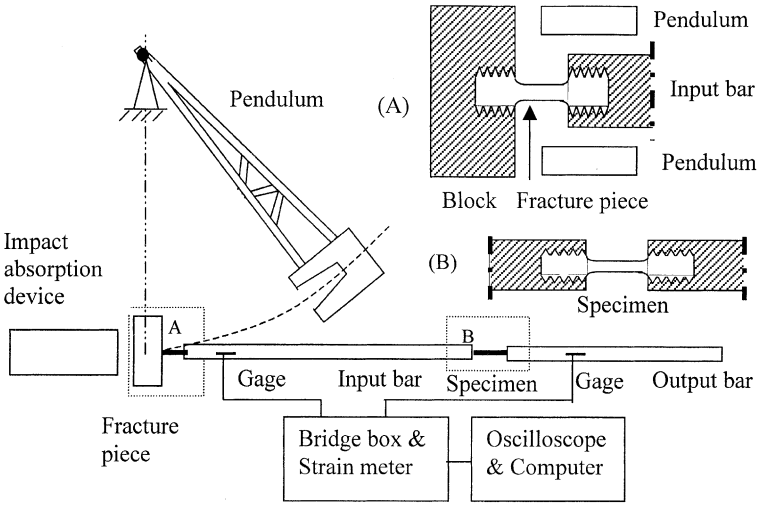

Fig. 1. Pendulum-driven tensile Kolsky bar and specimen.

used separately to independently record the input pulse, and the resulting signals compared. These tests showed that the individual signals from the gauge pairs were essentially identical, indicating the absence of flexural components. A metal block was connected to one end of the input bar via a fracture piece made of high-strength aluminum alloy (Fig. 1, (A)). A pendulum with a 1 m long arm and two parallel hammers at its free end, was used to strike two symmetrical points simultaneously on the metal block connected to the fracture piece. By this means, the fracture piece was stretched and made to generate a tensile pulse in the input bar. The fracture pieces were made of an aluminum alloy with relatively rate-independent properties (Nicholas, 1982), so that the magnitude of the input pulse was controlled only by the diameter of the piece and not the impact speed of the pendulum. The input pulse duration was primarily determined by the length and fracture strain of the fracture piece, as well as by the velocity of the striker. Since the fracture strain was constant, increasing the length of the fracture piece and decreasing the impact velocity of the striker resulted in an increase in the input pulse duration. Since the aluminum alloy used had negligible strain hardening, it stretched under an almost constant stress and this produced an approximately rectangular input wave.

If the diameter of the fracture piece was made sufficiently large, it would not attain fracture during impact and therefore, a tensile pulse of very long length could be generated. With the current arrangement, it was found that the maximum diameter at which the fracture piece broke was 5.5 mm. Fig. 2(a) shows a record of a typical incident and transmitted wave in a test on a titanium specimen. In this instance, the input wave experienced superposition by the wave reflected from the interface between the specimen and the input bar; this consequently truncated the input bar signal. The distance between the input strain gage and the specimen was about 2.3 m; based on a bar wave speed of 5130 ms^{-1}, the input tensile pulse had an effective duration of 897 μs, which was long enough to break the titanium specimens at strain rates between 100 and 1000 s^{-1}. An impact absorption device (Fig. 1) was incorporated to arrest the pendulum swing after impact.

The strain rate imposed on a test specimen, as determined by the amplitude of the incident wave, was varied by changing the diameter of the fracture piece. From the recorded incident $e_i(t)$ and transmitted $e_t(t)$ engineering strain signals in the bars (Fig. 2(a)), the engineering stress $s(t)$, strain $e(t)$ and strain rate $\dot{e}(t)$ in the specimen were determined from:

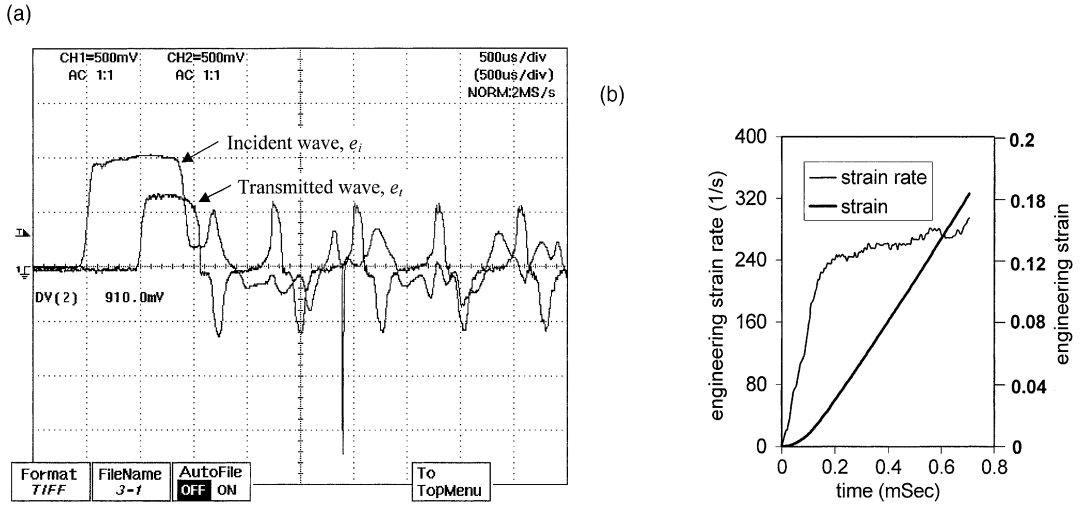

Fig. 2. (a) Incident and transmitted waves in a typical test and (b) variation of strain rate and strain with time.

$$s(t) = (A_0/A)E_0 e_t(t), \tag{1a}$$

$$e(t) = 2(c_0/L)\int_0^t [e_i(\tau) - e_t(\tau)]\,\mathrm{d}\tau, \tag{1b}$$

$$\dot{e}(t) = 2(c_0/L)[e_i(t) - e_t(t)], \tag{1c}$$

where E_0, A_0 and c_0 are respectively the Young's modulus, cross-sectional area and wave velocity of the bars, while A and L denote the cross-sectional area and length of the specimen. Fig. 2(b) shows the variation of strain rate and strain with time during the loading of a titanium test specimen and illustrates that the strain rate imposed using the SHPB apparatus was approximately constant. In the present study, a relatively long input pulse was required for Ti specimens to attain dynamic tensile fracture. Consequently, the strain gauge used to measure the input pulse was sited at a location sufficiently far away from the specimen (Fig. 1) to avoid superposition of the reflected wave from the bar–specimen interface. (This is an inherent potential problem in tensile SHPB tests.) The sufficiently small bar diameter, rise times of the elastic waves and wave propagation distances in the present SHPB apparatus were such that dispersion effects were insignificant. In an earlier work, Shim et al. (2001) examined this aspect in detail and other researchers (Noble et al., 1999; Staab and Gilat, 1991) have also successfully applied similar SHPB techniques to the dynamic tension of specimens without encountering significant wave dispersion.

As shown in Fig. 1, the specimen had threaded ends and was screwed into the bars. Unlike dynamic compression tests that usually involve non-threaded samples, the thread clearance and connection between the specimen and bars may introduce some errors in the results. To confirm that with the present experimental arrangement the potential error arising from this was negligible, a set of calibration tests was performed using specimens made of high strength AA6061 aluminum alloy, which like other high strength aluminum alloys, is rate-insensitive (Staab and Gilat, 1991; Nicholas, 1982; Dieter, 1988). Firstly, samples were subjected to quasi-static tension using an Instron universal testing machine, which induced a strain rate of 0.01 s^{-1}; next, specimens were loaded under tension at a strain rate of 600 s^{-1} using the Kolsky bar; finally, strain gages were bonded onto the specimens to measure the strain directly. Stress–strain curves obtained from static and dynamic tests (computed using Eq. (1a)–(1c) and also from the directly measured

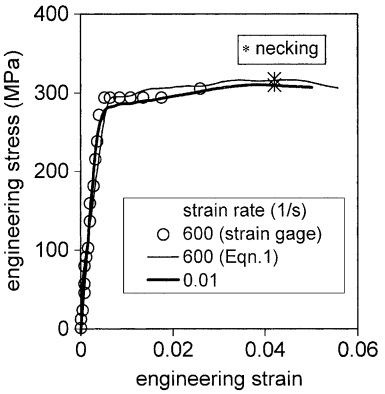

Fig. 3. Comparison between static and dynamic stress–strain curves for aluminum alloy.

strain signal) were compared to ascertain similarity. Fig. 3 shows this comparison and demonstrates that the static and dynamic responses in terms of engineering stress and strain were essentially identical, thus confirming that the threaded connection between the specimen and the input/output bars did not introduce appreciable error.

2.2. Tests on titanium samples

The titanium under investigation was commercially pure Grade 2 α-titanium and its chemical composition is given in Table 1. Specimens of a dumb-bell geometry, 9 mm in diameter and with a gauge length of 54 mm, were fabricated for static tests, in compliance with ASTM E-8M-97 standards for measuring the response of high-strength materials at large plastic strains. Specimens of 2 mm diameter and 9 mm gauge length (Fig. 1) were used in dynamic tests conducted on a pendulum-driven tensile Kolsky bar. Three samples were tested at each strain rate, ranging from 250 to 1100 s^{-1}. The elastic, yield and failure parameters which characterize the material are presented in Table 2, which summarizes both static and dynamic results.

Table 1
Chemical composition of Grade 2 α-titanium

Element	C	Fe	N	O	H	Ti
Wt.%	0.01	0.07	0.01	0.14	<0.001	Balance

Table 2
Summary of test results for Grade 2 α-titanium

Strain rate (s^{-1})	Number of samples	Young's modulus (GPa)	Yield stress (MPa)	UTS (MPa)	% Engineering strain at UTS (uniform true strain)	% elongation
0.01	3	112.5	347	474	15.5 (14.5)	42.3
250	3	NA	521	555	10.5 (9.98)	19.1
400	3	NA	533	560	10.4 (9.89)	19.5
650	3	NA	541	584	10.6 (10.1)	19.7
1100	3	NA	575	604	10.7 (10.2)	19.0

3. Test results and discussion

3.1. Flow stress behavior

Quasi-static and dynamic tensile engineering stress–strain curves for Grade 2 α-titanium, for strain rates ranging from 10^{-2} to 10^{3} s^{-1} are presented in Fig. 4(a). Assuming both constancy of volume and a homogeneous distribution of strain along the gage length of the specimens, true stress–strain curves are depicted in Fig. 4(b). The dashed lines after necking in the true stress–strain curves are approximations, because strain concentrates in the neck and the material continues to strain-harden all the way up to fracture. Rate-sensitivity is quantified in Fig. 5, which depicts the true flow stress (at a true strain of 6%) as a function of strain rate. Figs. 4 and 5, as well as Table 2, clearly show that the effective flow stress increases with strain rate, and that there is noticeable strain hardening under both static and dynamic loading. The flow stress increases by about 120 MPa as the strain rate is increased from quasi-static conditions to about 1100 s^{-1}. These results agree with those for similar materials (Chichili et al., 1998; Harding, 1975). For strain rates ranging from 250 to 1100 s^{-1}, this material exhibits a linear relationship between the flow stress and the logarithm of the strain rate. When compared with static response, the dynamic curves show similar strain hardening characteristics.

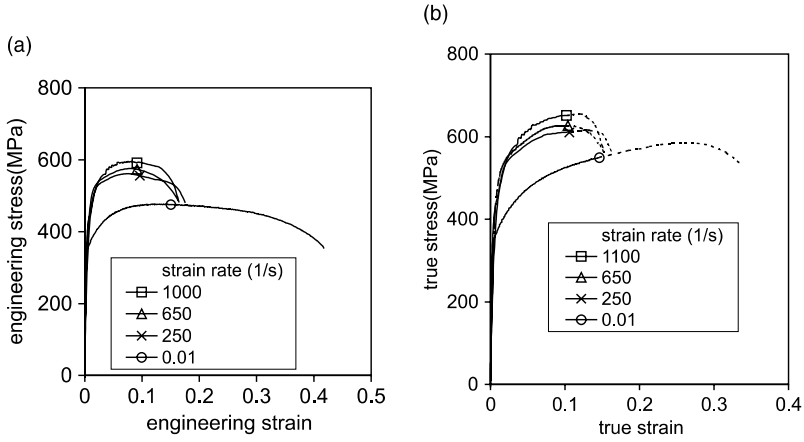

Fig. 4. (a) Engineering and (b) true stress–true strain curves for Grade 2 α-titanium.

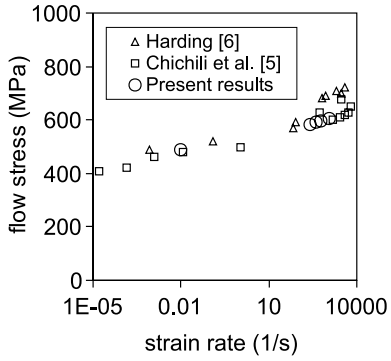

Fig. 5. Variation of flow stress with strain rate at 6% strain for Grade 2 α-titanium.

3.2. Dynamic tensile instability

Based on the assumption of a uniformly distributed strain, Fig. 4(a) and Table 2 show that the engineering strain at UTS under dynamic loading is about 68% of that under static loading. The values of uniform true strain provided in parentheses in Table 2, are useful in estimating the formability of metals from the results of tension tests. The mechanism associated with the decrease in necking strain for dynamic tension remains to be fully examined. Rapid, high-rate experiments are nearly completely adiabatic and the heat converted from plastic work during deformation raises the specimen temperature. Hence, both strain rate and temperature effects must be taken into account for such deformation analysis.

Necking initiates at the onset of tensile instability, whereby the increase in strength due to strain hardening fails to compensate for the decrease in cross-sectional area (Dieter, 1988). At the point of tensile instability:

$$\mathrm{d}\sigma/\mathrm{d}\varepsilon = \sigma, \tag{2}$$

where σ and ε are the true stress and true strain.

For a deformation process at a constant high strain rate, the general constitutive relationship is assumed to take the form:

$$\sigma = \sigma(\varepsilon) = f(\varepsilon)g(\dot{\varepsilon})h(T(\varepsilon)), \tag{3}$$

where f represents the stress–strain relationship at a reference strain rate, normally associated with quasi-static loading; g defines the influence of strain rate; h represent the influence of temperature change due to plastic work. Previous researchers (Dieter, 1988; Mason et al., 1994) have concluded that around 90% or more of the energy expended in plastic deformation is converted to heat. Recently, Kapoor and Nemat-Nasser (1997) reported that within experimental error, close to 100% of the work done during high strain rate deformation is converted to heat. Rapid, high-rate deformation is nearly completely adiabatic; therefore, it is reasonable to assume that all the plastic work done is converted to heat and thus the specimen temperature rise is:

$$\mathrm{d}T = \frac{\sigma \mathrm{d}\varepsilon}{\rho c}, \tag{4}$$

where ρ (4.51 g/cm^3 for α-titanium) and c (0.518 J/g/K for α-titanium at room temperature) are the density and constant-volume heat capacity.

From Eqs. (2)–(4), tensile instability or necking under dynamic tension at a constant strain rate ($\mathrm{d}\dot{\varepsilon}/\mathrm{d}\varepsilon = 0$) initiates when:

$$\frac{\mathrm{d}\sigma}{\mathrm{d}\varepsilon} = gh\frac{\mathrm{d}f}{\mathrm{d}\varepsilon} + gf\frac{\mathrm{d}h}{\mathrm{d}T}\frac{\mathrm{d}T}{\mathrm{d}\varepsilon} = fgh, \tag{5a}$$

i.e.

$$\frac{\mathrm{d}f}{\mathrm{d}\varepsilon} + \frac{gf^2}{c\rho}\frac{\mathrm{d}h}{\mathrm{d}T} = f, \tag{5b}$$

$$\frac{f'(\varepsilon)}{f^2(\varepsilon)} - \frac{1}{f(\varepsilon)} + \frac{g(\dot{\varepsilon})}{c\rho}h'(T) = 0 \tag{6a}$$

or

$$\frac{\mathrm{d}f(\varepsilon)}{\mathrm{d}\varepsilon} = f(\varepsilon) - f^2(\varepsilon)\frac{g(\dot{\varepsilon})}{c\rho}\frac{\mathrm{d}h(T)}{\mathrm{d}T}. \tag{6b}$$

Compared with the expression governing necking under static loading,

$$\frac{\mathrm{d}f(\varepsilon)}{\mathrm{d}\varepsilon} = f(\varepsilon). \tag{7}$$

Eq. (6b) shows the influence of strain rate $(g(\dot{\varepsilon}))$ and temperature softening $(h(T))$ on tensile instability. In the absence of thermal softening, i.e. $h'(T) = 0$ or $h(T) =$ constant (temperature-independent materials or isothermal deformation), the strain at UTS (necking strain) under dynamic tension is the static response value. With respect to the second term on the right-hand side of Eq. (6b), $g(\dot{\varepsilon})$ is a positive quantity. The temperature term $h(T)$ is also positive, but its derivative $h'(T)$ is negative; it is well-known that the influence of temperature on the flow stress of metals (strain and strain-rate remaining constant) is of the form $\sigma = A\mathrm{e}^{-RT/Q}$, where A is a constant, R is the universal gas constant and Q the plastic flow activation energy (e.g. Dieter, 1988). The derivative of a function of this form with respect to temperature is thus negative. Consequently, the right-hand side of Eq. (6b) is larger than that of Eq. (7). A combination of this with the fact that the stress–strain curve of strain-hardening metals $f(\varepsilon)$ increases monotonically, but its tangent modulus $\mathrm{d}f(\varepsilon)/\mathrm{d}\varepsilon$ decreases with strain, shows that the solution of Eq. (6b) will yield a smaller value of strain than Eq. (7); i.e. a greater rate and temperature sensitivity results in a reduction of the necking strain.

3.3. Analysis of dynamic tensile instability

In order to evaluate the influence of strain rate and temperature on the necking strain under dynamic tension, the Johnson–Cook model (Johnson and Cook, 1983) is assumed:

$$\sigma = (A + B\varepsilon^n)\left(1 + C\ln\frac{\dot{\varepsilon}}{\dot{\varepsilon}_0}\right)\left[1 - \left(\frac{T - T_\mathrm{r}}{T_\mathrm{m} - T_\mathrm{r}}\right)^m\right], \tag{8}$$

where σ, ε and $\dot{\varepsilon}$ are respectively the flow stress, plastic strain and plastic strain rate; $\dot{\varepsilon}_0$ ($= 0.01\ \mathrm{s}^{-1}$ at static loading) is the reference strain rate; T, T_r ($= 298$ K room temperature) and T_m ($= 1940$ K for α-titanium) are respectively the current, reference and melting temperatures; A, B, C, n and m are material constants determined experimentally. In line with previous treatment of the Johnson–Cook model (Johnson and Cook, 1983; Nemat-Nasser et al., 1994; Rule, 1997), elastic strain is neglected and the plastic strain in Eq. (8) is assumed to be the total true strain.

Fig. 6 shows how the temperature rises with true plastic strain in α-titanium during dynamic tension; the temperature rise is evaluated by integrating Eq. (4) with respect to experimental true stress–strain curves.

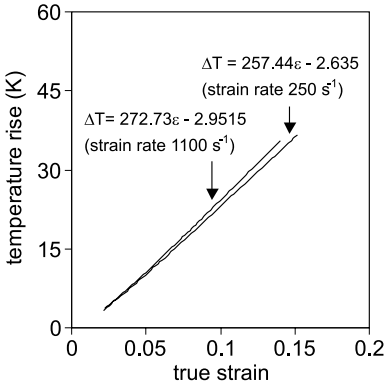

Fig. 6. Variation of temperature rise with strain at high strain rates for Grade 2 α-titanium.

Experimental results from the present study show that necking occurs at a true strain of 10%, when a specimen is stretched at a strain rate of 1100 s^{-1}. Fig. 6 shows that at a strain of 10% and a strain rate of 1100 s^{-1}, the temperature rise is only about 23 K (the specimen temperature increases to 321 K), which is not a significant change compared with the melting temperature of titanium alloy (1940 K). The relationship between temperature rise ($\Delta T = T - T_r$) and strain can be expressed as:

$$\Delta T = 257.44\varepsilon - 2.635 \quad (\dot{\varepsilon} = 250\ s^{-1},\ 0.02 < \varepsilon < 0.16), \tag{9a}$$

$$\Delta T = 272.73\varepsilon - 2.9515 \quad (\dot{\varepsilon} = 1100\ s^{-1},\ 0.02 < \varepsilon < 0.16). \tag{9b}$$

For the same strain range, a fit for the static true stress–strain curve using Eq. (8) results in $A = 0$, $B = 725.2$ and $n = 0.1434$. The fitted curve is shown in Fig. 7. Curve fits for Eq. (8) with the data in Figs. 4(b) and 5 yield a value of $C = 0.025$.

Hence, the only undetermined parameter in Eq. (8) is m. By combining Eqs. (8) and (2), variation of the necking strain with the temperature parameter m, for dynamic tension at 250 and 1100 s^{-1}, is determined numerically and shown in Fig. 8. Within this range of strain rates tested range (250–1100 s^{-1}), a value of $m = 0.75$ is found to provide the best fit. Note that m is the only parameter in the J–C model that defines the influence of thermal softening in metals under dynamic loading. When m is smaller than 1, there is a sharp

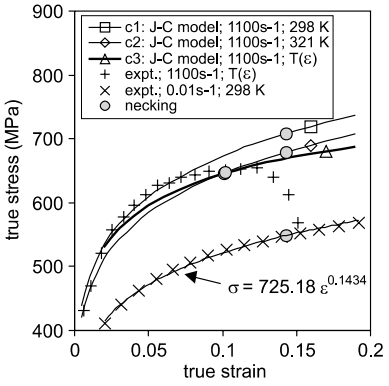

Fig. 7. Influence of strain rate and temperature on the strain at UTS for Grade 2 α-titanium.

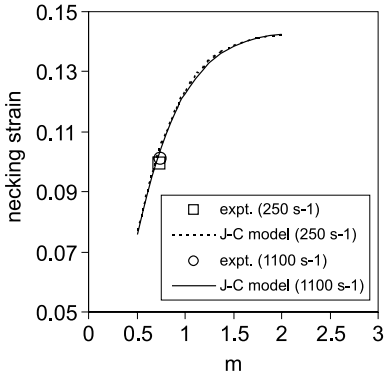

Fig. 8. Variation of necking strain under dynamic tension with temperature parameter m for Grade 2 α-titanium.

decrease in the necking strain (Fig. 8), indicating that the influence of thermal softening on necking is significant. Consequently, for this class of metals ($m < 1$), dynamic tension is possibly a better means to determine the value of m when compared with other approaches such as Taylor bar impact (Rule, 1997).

Fig. 7 also shows how strain rate and temperature influence necking under dynamic tension. Curves c1 and c2 are respective isothermal dynamic stress–strain curves based on Eq. (8) with $\dot{\varepsilon} = 1100\ s^{-1}$ at temperatures of $T = 278$ K (RT) and $T = 321$ K (specimen temperature at necking based on applying Eq. (4) to the experimental results). As expected, they produce the same values for the necking strain as that under static loading. Curve c3 is the actual experimental (adiabatic) dynamic stress–strain curve ($\dot{\varepsilon} = 1100\ s^{-1}$) which includes the effects of thermal softening ($T = T(\varepsilon)$). It is noted that the initial portion of the curve follows that of c1 (isothermal, RT response) and then deviates downwards to intersect c2 (isothermal at 321 K). This appears to indicate that softening sets in when sufficient adiabatic heating occurs. Consequently, a much lower necking strain is also observed. Based on the Johnson–Cook model, it can be seen that a change in temperature of 23 K can decrease the necking strain by 30% for α-titanium under high rate loading ($1100\ s^{-1}$). The preceding analysis uses results from experimental tests on specimens of one size and assumes that these specimens represent the dynamic behavior of the bulk material. Knoche and Needleman (1993) employed finite element modeling to examine the effects of specimen size on dynamic tensile failure of metals. Their results indicate that there is some variation in failure initiation with specimen size. However, the influence of specimen size on necking strain is not a consideration in the present study.

The present results show that Grade 2 α-titanium is both strain rate and temperature sensitive, the former enhancing the tensile flow stress, while the latter decreasing it. Adoption of the Johnson–Cook model yields a temperature parameter m of 0.75. This corresponds to a decrease of 30 MPa in flow stress at $\varepsilon = 14.3\%$ and $\dot{\varepsilon} = 1100\ s^{-1}$, due to an increase of 23 K in temperature. In contrast, AA6061 aluminum alloy shows no decrease in necking strain under dynamic tension, compared with its static response (Fig. 3). This is because the material is insensitive to both strain rate and temperature in the test range. A comparison of the current findings can be made with those by Kapoor and Nemat-Nasser (1997), who subjected 6061 aluminum alloy to dynamic deformation (via compression) and found that its dynamic flow stress is also insensitive to temperature increases. Similarly, their tests on dynamic compression of commercially pure titanium exhibited a decrease in flow stress by 70 MPa (at $\varepsilon = 20\%$ and $\dot{\varepsilon} = 3000\ s^{-1}$), arising from a temperature rise of 33 K.

3.4. Fracture behavior

Fig. 9 depicts specimens fractured under static and dynamic tension. It shows the occurrence of necking before fracture and the similarity of neck geometry for both static and dynamic loading. A cup-and-cone-type ductile fracture surface was found for both static and dynamic loading. Microscopic examination revealed a dimpled rupture surface characterized by cup-like depressions, which denotes ductile fracture.

The values of percentage elongation for static and dynamic loading are listed in Table 2. The measured elongation from a tension specimen depends on its gage length and the cross-sectional dimensions. This is because the total extension consists of two components, uniform extension prior to necking and localized extension after necking begins. However, it is generally recognized that if specimens are geometrically similar, elongation measurements of different-sized specimens can be compared. For cylindrical specimens, this means that the ratio of the gage length (L_0) to the initial diameter (D_0) must be maintained (Dieter, 1988). In this study, the specimens used for static and dynamic tests are different in size, but the ratio $L_0/D_0 = 4.5$ is kept constant. Therefore, values of the percentage elongation in Table 2 can be compared with one another. Table 2 shows a decrease of about 50% in percentage elongation under dynamic loading; this is less severe than the decease in necking strain (68%).

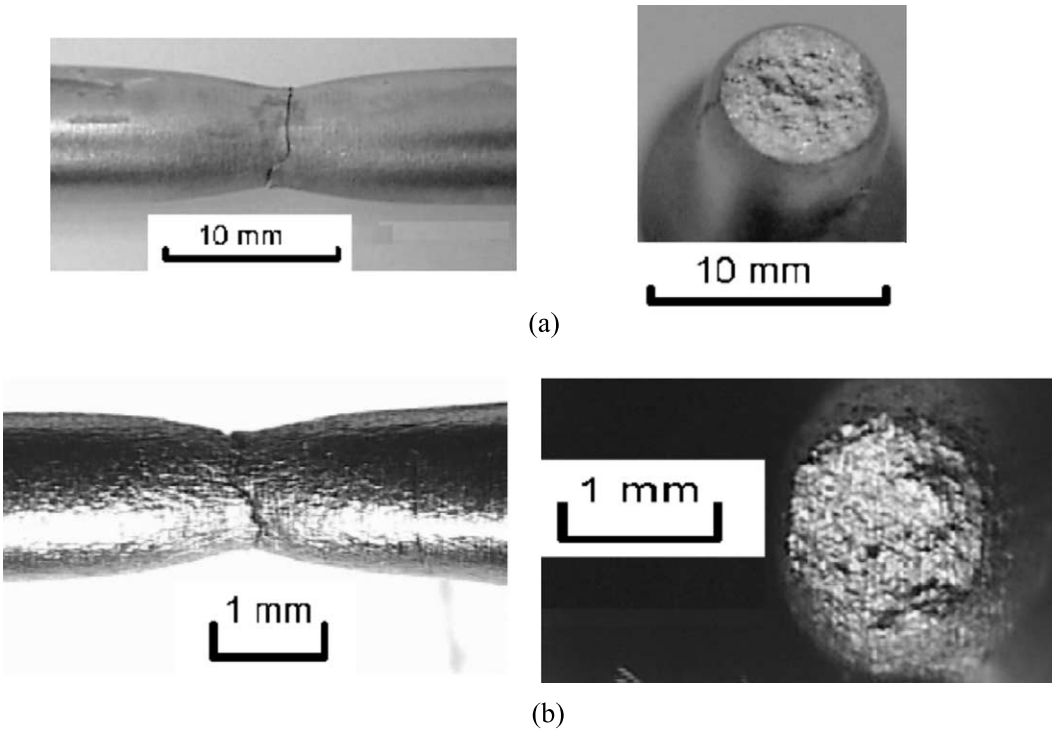

Fig. 9. Fracture in Grade 2 α-titanium specimens under (a) static and (b) dynamic tension.

4. Conclusions

(1) Tensile pulses of sufficiently long duration to induce fracture in ductile specimens, can be generated by incorporating a sacrificial fracture piece of adequately large diameter into a pendulum-driven tensile Kolsky bar. This arrangement facilitates investigation into the dynamic response of ductile materials at moderately high strain rates.

(2) Dynamic calibration tests using rate-independent aluminum alloy specimens with strain gages bonded directly on them, show that threaded connections between the specimen and the input/output bars do not introduce appreciable error.

(3) The tensile behavior of Grade 2 α-titanium under static loading and at moderately high strain rates (200–1000 s^{-1}) was characterized. Results show that the flow stress increases with strain rate and strain hardening occurs over the range of strain rates investigated. The material exhibits ductile fracture.

(4) Necking in α-titanium occurs much earlier at high stain rates and results in a significantly smaller necking strain. An Eq. (6a) and (6b), defining the condition for necking in terms of strain rate and temperature softening has been derived. There is a decrease in the necking strain arising from adiabatic thermal softening under high rates of strain. For dynamic tension at a strain rate of 1100 s^{-1}, adiabatic heating generates a temperature rise of 23 K, while strain rate sensitivity results in a flow stress increase of 128 MPa. These two effects produce a decrease of 30% in the necking strain. It was found that the Johnson–Cook model is able to capture both the rate and temperature dependent behavior of α-titanium adequately.

References

Chichili, D.R., Ramesh, K.T., Hemker, K.J., 1998. The high-strain-rate response of alpha-titanium: experiments, deformation mechanisms and modeling. Acta Mater. 46 (3), 1025–1043.

Dieter, G.E., 1988. Mechanical Metallurgy. McGraw-Hill, Singapore.

Harding, J., 1975. The Temperature and strain rate sensitivity of α-titanium. Arch. Mech. 27, 715–732.

Harding, J., Welsh, L.M., 1983. A tensile testing technique for fiber-reinforced composites at impact rates of strain. J. Mater. Sci. 18, 1810–1826.

Johnson, G.R., Cook, W.H., 1983. A constitutive model and data for metals subjected to large strains, high strain rate, and high temperatures. In: Proc. 7th Int. Symp. On Ballistics. ADPA, The Netherlands, pp. 1–7.

Kailas, S.V., Prasad, Y.V.R.K., Biswas, S.K., 1993. Microstructural features of flow instability in a-titanium cylinders under high strain rate compression at 25 °C to 400 °C. Metall. Trans. 24A, 2513–2520.

Kailas, S.V., Prasad, Y.V.R.K., Biswas, S.K., 1994a. Influence of initial texture on the microstructural instabilities during compression of commercial α-titanium at 25 °C to 400 °C. Metall. Trans. 25A, 1425–1434.

Kailas, S.V., Prasad, Y.V.R.K., Biswas, S.K., 1994b. Flow instabilities and fracture in Ti–6Al–4V deformed in compression at 298 K to 673 K. Metall. Trans. A 25, 2173–2179.

Kapoor, R., Nemat-Nasser, S., 1997. Determination of temperature rise during high strain rate deformation. Mech. Mater. 27, 1–12.

Kawata, K., Hashimoto, S., Kurokawa, K., Kanayama, N., 1979. A new testing method for the characterization of materials in high velocity tension. In: Mechanical Properties at High Rates of Strain. Institute of Physics, Bristol and London, pp. 71–80.

Knoche, P., Needleman, A., 1993. The effect of size on the ductility of dynamically loaded tensile bars. Eur. J. Mech. A—Solids 12 (4), 585–601.

Kolsky, H., 1949. An investigation of the mechanical properties of materials at very high rates of loading. Proc. Phys. Soc. London 62B, 676–700.

Lindholm, U.S., Yeakley, L.M., 1981. High strain-rate testing: tension and compression. Exp. Mech. 8 (1), 1–9.

Mason, J.J., Rosakis, A.J., Ravichandran, G., 1994. On the strain and strain rate dependence of the fraction of plastic work converted to heat: an experimental study using high speed infrared detectors and the Koslky bar. Mach. Mater. 17, 135–145.

Meyers, M.A., Subhash, G., Kad, B.K., Prasad, L., 1994. Evolution of microstructure and shear-band formation in alpha-HCP titanium. Mech. Mater. 17, 175–193.

Nemat-Nasser, S., Li, Y-F, Isaac, J.B., 1994. Experimental/computational evaluation of flow stress at high strain rates with application to adiabatic shear banding. Mech. Mater. 17, 111–134.

Nicholas, T., 1981. Tensile testing of materials at high rates of strain. Exp. Mech. 21 (5), 177–185.

Nicholas, T., 1982. Material behavior at high strain rates. In: Impact Dynamics. Wiley, New York, pp. 277–332.

Noble, J.P., Goldthorpe, B.D., Church, P., Harding, J., 1999. The use of the Hopkinson bar to validate constitutive relations at high rates of strain. J. Mech. Phys. Solids 47, 1187–1206.

Rule, W.K., 1997. A numerical scheme for extracting strength model coefficients from Taylor test data. Int. J. Impact Engng. 9–10 (19), 797–810.

Staab, G.H., Gilat, A., 1991. A direct-tension split Hopkinson bar for high strain-rate testing. Exp. Mech. 31 (3), 232–235.

Shim, V.P.W., Yuan, J., Lee, S.-H., 2001. A technique for rapid two-stage dynamic tensile loading of polymers. Exp. Mech. 41 (1), 122–127.